DOI 10.31489/2023PH3/107-118

UDC 538.9;621.383

T.M. Mukametkali[1], X.S. Rozhkova[1], A.K. Aimukhanov[1], B.R. Ilyassov[2], K. Apshe[1], A.K. Zeinidenov[1*]

[1] Karaganda University of the name of academician E.A. Buketov, Scientific Center of nanotechnology and functional nanomaterials, Karaganda, Kazakhstan;
[2] Astana IT University, Expo C1, Astana, Kazakhstan
([*]E-mail address: a.k.zeinidenov@gmail.com)

The effect of the $CH_3NH_3PbCl_xI_{3-x}$ perovskite layer thickness and grain size on its electrophysical and optical properties

Lead halide perovskite $CH_3NH_3PbCl_xI_{3-x}$ thin films are widely used as photoactive layers in perovskite solar cells. $CH_3NH_3PbCl_xI_{3-x}$ is a low band gap semiconductor with a broad absorption spectrum and a high conductivity showing excellent compatibility with exciting hole and electron selective layers in terms of electronic energy alignment, which provide efficient charge generation, separation and transport in perovskite solar cells. In this paper, $CH_3NH_3PbCl_xI_{3-x}$ layers were deposited on the TiO_2 surface by one step spin-coating technique from a methylammonium iodide (MAI) and lead chloride ($PbCl_2$) solution. To prepare the perovskite solution, $PbCl_2$ (Sigma-Aldrich)230 mg of $PbCl_2$ and 394 mg of MAI were dissolved in 1 ml of N, N-Dimethylformamide (Sigma-Aldrich) solvent. As expected, the elevation of the spin-coating rate resulted in $CH_3NH_3PbCl_xI_{3-x}$ thickness reduction, which should lead to a decrease in the R_3 resistance in $CH_3NH_3PbCl_xI_{3-x}$. However, the impedance spectroscopy revealed that with thickness reduction from 955 nm to 753 nm, the R_3 resistance of $CH_3NH_3PbCl_xI_{3-x}$ declines from about 2590 Ω to 2258 Ω reaching the minimum value at 505 nm. The further decrease in $CH_3NH_3PbCl_xI_{3-x}$ thickness increased $CH_3NH_3PbCl_xI_{3-x}$ film resistance. The study of $CH_3NH_3PbCl_xI_{3-x}$ absorbance and luminescence spectra showed that the change in $CH_3NH_3PbCl_xI_{3-x}$ defect density occurred, which explains the decrease in $CH_3NH_3PbCl_xI_{3-x}$ resistance. According to the absorbance and luminescence spectroscopy study, the $CH_3NH_3PbCl_xI_{3-x}$ thickness reduction led to a decrease in the density of interstitial $CH_3NH_3PbCl_xI_{3-x}^+$ defects. $CH_3NH_3PbCl_xI_{3-x}^+$ species form deep levels trapping free electrons and as a result, increasing $CH_3NH_3PbCl_xI_{3-x}$ resistance. The PSCs based on a 505 nm thick $CH_3NH_3PbCl_xI_{3-x}$ layer showed the highest performance with the improved short current density and fill factor. The champion device had a power conversion efficiency of 9.92 %.

Keywords: Perovskite solar cells, photoactive layer, $CH_3NH_3PbCl_xI_{3-x}$, copper phthalocyanine, iodine ions, impedance meter, electron transport layer, hole transport layer.

Introduction

Organic-inorganic metal halide materials with a perovskite structure are at the stage of intensive studies. Hybrid perovskites are direct-gap semiconductors with a unique set of optical and electronic properties, which makes them practically ideal materials for photovoltaics and optoelectronics. The power conversion efficiency (PCE) of perovskite solar cells (PSCs) has reached 25.7 % [1]. The high PCE in combination with inexpensive fabrication methods makes PSCs the most promising devices for modern photovoltaics. They have become the main competitor to traditional inorganic solar cells [2].

Organic-inorganic metal halide perovskites have bipolar conductivity, which allows effective transport and separation of electrons and holes at perovskite/electron transport layer (ETL) and perovskite/hole transport layer (HTL) interfaces. The electronic energy level consistency at the interface perovskite/charge selective layer (ETL and HTL) plays crucial role for the efficient extraction of charge carriers from the perovskite.

For effective hole extraction, VBM (valence band maximum) level in HTL should be slightly higher than VBM level in the perovskite. In addition, a higher position of CBM (conduction band minimum) level in HTL relative to CBM level in the perovskite blocks electrons and prevents electron transport to the anode [3, 4]. Recent studies have shown that the charge transfer properties at the perovskite/HTL interface are a major factor limiting the efficiency and stability of PSCs [3].

In recent years, improvements in the crystallinity and morphology of the perovskite layers have led to further boost in PCE of PSCs. However, more deep and advanced studies are still needed to optimize charge transfer processes in PSCs in order to minimize charge recombination, eliminate hysteresis and to increase device stability. The perovskite layer's crystallinity, uniformity, roughness and thickness are critical

parameters to control during the film deposition. Obtaining uniform, smooth and pin-holes and crack free perovskite layer are necessary to fabricate high efficient devices. Currently there are two solution processable deposition techniques of perovskite thein films: one step and two-step sequential deposition techniques. Perovskite thin films deposited by the one-step method have large grains, however the film surface is rough and they have relatively high defect density [4]. Kim et al. demonstrated a two-step sequential deposition method, which can alleviate challenges inherent the one-step methods. PSCs fabricated by Kim et al. showed PCE of around 15 % [5]. Except, the solution processable methods, there are other deposition methods, which also demonstrates high efficient PCSs. The Liu et al. reported planar PCSs with PCE of 15.4 % where refers to uniform perovskite layers were deposited by a sputtering technique [6]. It is very easy to study the morphology of the thin film.

The morphology and structure of the perovskite thin films are very sensitive to the synthesis conditions, such as nature of precursors and solvents, deposition and annealing temperature and environment, and a deposition rate [4-7]. Recently, highly smooth perovskite thin films with high crystallinity were obtained by annealing in mixed solvent vapor at room temperature, and PCSs showed PCE of 16.4 % [8]. In 2015, Ko et al. reported PCSs with PCE up to 15.76 % by keeping the substrate temperature at the range of 40 °C-60 °C to control the perovskite layer crystallization [9]. All of these studies imply that the crystallinity and morphology of the perovskite layers are very important to fabricate high-performance solar cells.

In the last few years, record PCE of PSCs has increased from 3.8 % to more than 20 % [7-11]. Compared to other types of solar cells, PCSs have many promising advantages. Compared to silicon-based solar cells, the mass production cost of PSCs will be lower. At the same level of energy conversion efficiency, HPSCs cost only 1/20th the cost of silicon-based solar cells. Currently, record efficiency of PSCs is 25.2 %, which is close to the efficiency of silicon-based solar cells (~27.1 %), and PCE as high as 30 % are predicted for them [10].

With the great efforts of researchers and engineers around the world, PCSs efficiency has now set a record for thin-film solar cells. Structure engineering, morphology optimization and interface modification have been the main research focus to ensure the high efficiency of PSC [8-10]. The morphology and degree of crystallinity of the perovskite films were found to be crucial factors for the development of highly efficient and stable solar cells [11]. The main goal of optimization studies is to deposit highly crystalline perovskite films with large grains and pin-holes free. This is accomplished by optimizing deposition conditions: solution concentration and temperature, drying and annealing conditions [12-14]. In this paper, we also demonstrate the importance of obtaining high-quality perovskite thin films by optimizing crystallization process. Because the morphology of the perovskite absorber thin film is one of the most important factors affecting the overall power, and conversion efficiency of perovskite solar cells [15-16]. To improve the homogeneity of the film, efforts are made to improve the crystallization of the perovskite shell, and these processes should be well understood and studied [17-20].

Methods of making perovskite thin films with low cost, easy energy conversion, quick preparation, and easy application have been studied [21-22]. Therefore, the preparation methods are optimized for growing larger perovskite crystals, improving a homogeneous and pore-free thin film and a closer arrangement of crystal grain boundaries for better interfacial bonding. In this research paper, we investigated the optimization of perovskite morphology to achieve highly efficient and stable perovskite solar cells.

In this work, we optimize the deposition conditions of $CH_3NH_3PbCl_xI_{3-x}$layers, and in addition, study the effect of double hole transport layers based on CuPc and MoO_3 on PSCs performance. The use of CuPc and MoO_3 as HTLs in PSCs will significantly reduce the cost of perovskite solar panels. The optimization and using double HTL led to enhanced absorption and significantly the growth of the current density. The champion device revealed PCE as high as 9.92 %.

Materials and Methods

Sample preparation and deposition process

Solar Cell Fabrication. Perovskite solar cells were fabricated on glass substrates coated with an FTO layer (15 Ohm/cm^2). FTO serves as an external electrode (cathode). First, substrates were thoroughly cleaned in acetone, hot deionized water, and 2-proponal followed by UV-ozone treatment. For the electron transport layer, a TiO_2 sol-gel solution prepared, at first, 15 mL of the aqueous solutions of titanium VI isopropoxide(TTIP)(Ti[$OCH(CH_3)_2$]$_4$ 99.999 % purity, Sigma-Aldrich, USA) was slowly added to 30 mL of acetic acid (HCOOH 99.9 % purity, Sigma-Aldrich, USA) in a three-neck flask, and the mixture was stirred for 5 minutes to avoid agglomeration. The mixture of deionized water (4 mL) and isopropanol

($CH_3CH(OH)CH_3$ 99.9 %, Sigma-Aldrich, USA) (15 mL) was added dropwise to the solution and then stirred vigorously for another 10 minutes. After mixing the solution, 4 mL of nitric acid (HNO_3) was added to the solution as a stabilizer, and the mixture was further subjected to vigorous stirring for 20 minutes. TiO_2 Nano solution formed from the hydrolysis and condensation reactions of titanium Alco oxide precursors. In the presence of water, titanium Alco oxide hydrolyzed and subsequently polymerized to form 3-dimensional TiO_2 nanoparticles, which dispersed on the FTO glass substrates and spun at 5000 rpm. Further, the spin-coated pre-TiO_2 film was annealed at a temperature of 500℃ for 60 minutes to obtain crystalline a TiO_2 layer.

Perovskite Materials. In the next step, a photoactive perovskite layer was deposited on the TiO_2 surface by one step spin-coating technique from a methylammonium iodide (MAI) and lead chloride ($PbCl_2$) solution. To prepare the perovskite solution, $PbCl_2$ (Sigma-Aldrich)230 mg of $PbCl_2$ and 394 mg of MAI were dissolved in 1 ml of N, N-Dimethylformamide (Sigma-Aldrich) solvent. The resulting solution was stirred on a magnetic stirrer at 70 °C for 2 hours to get a uniform solution. The perovskite solution was spin-coated at 2000, 3000, 4000, 5000, and 6000 rpm. The perovskite layer was annealed for 2 hours at a temperature of 90 °C to form a crystalline perovskite layer. The crystallization process was accompanied by a change in the color of the film from yellow to dark brown. All steps including perovskite formation carried out in a glove box filled with nitrogen.

Composition of HTM. After the perovskite layer formation step was done, copper phthalocyanine (CuPc) serving as a hole transport layer (HTL) was deposited on the perovskite surface. HTL with a thickness of 80 nm was deposited by thermal evaporation of CuPc powder (Sigma-Aldrich) at a vacuum level of 10^{-3} Pa. Further, a 30 nm MoO_x layer was thermally evaporated from MoO_3 (Borun New Material Technology Co., Ltd.) on the CuPc surface at the vacuum level of 10^{-2} Pa. Finally, an Ag electrode (anode) with a thickness of 100 nm thermally evaporated at a vacuum of 10^{-3} Pa.

Structural formulas of CuPc, MAI, and $PbCl_2$, a diagram of perovskite solar cell fabrication steps (b), and PSCs structure with functional layers' energy diagrams are shown in Figure 1.

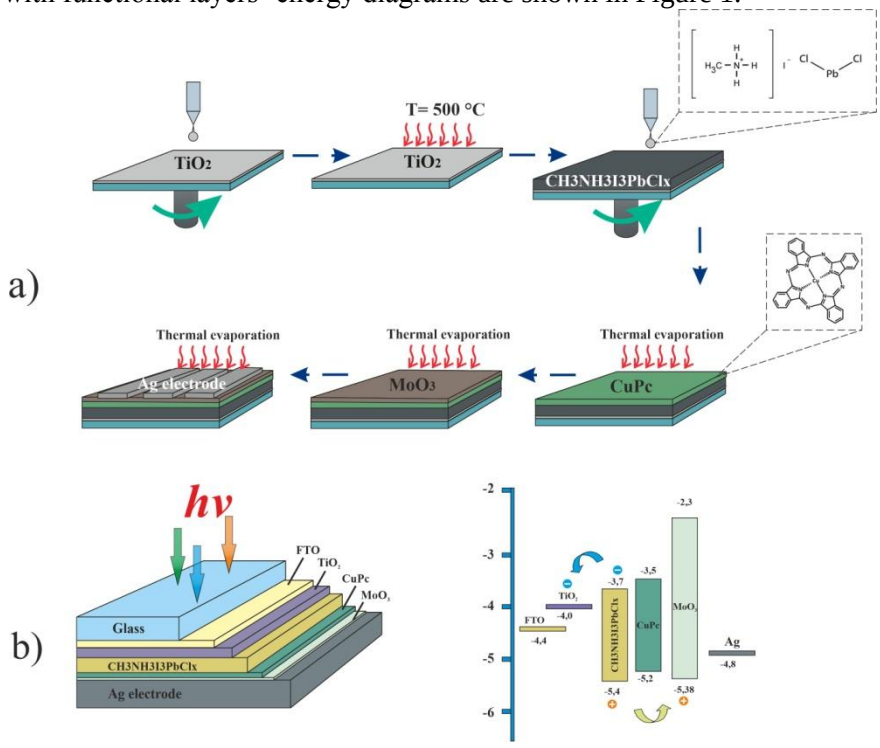

Figure 1. Structural formulas (a), a scheme of perovskite solar cell fabrication steps (b) and PSCs structure with functional layers' energy diagrams

Analysis methods

The surface topography and thickness of the samples were probed by a JEOL JSPM-5400 atomic force microscope (AFM). The AFM data were processed by Gwyddion Data-Processing Software, a modular program for SPM (scanning probe microscopy) data visualization and analysis. To measure the local current

distribution, an AFM SolverP47 (NT-MDT) was used. When measuring the current, a voltage was applied to the sample, while the conductive probe covered with a gold film was grounded. The surface topography and surface standard deviation (rms) were measured in the semi-contact mode (NSC14 probe, Micromash), and the current was measured in the contact mode (CSC37/Au probe, Micromash).

The thickness of the deposited PSCs layers was measured using a scanning electron microscope (SEM, MIRA 3 LMU, Tescan).

The absorption spectra of the samples were measured by an AvaSpec-ULS2048CL-EVO spectrometer (Avantes). A combined deuterium-halogen light source AvaLight-DHc (Avantes) with an optical range of 200–2500 nm was used as a light source.

For thermal deposition, the CY-1700x-spc-2 vacuum sputtering unit (Zhengzhou CY Scientific Instruments Co., Ltd) was used.

The photoluminescence decay kinetics was measured on a pulsed spectrofluorometric with picosecond resolution and registration in the photon-counting mode.

The impedance spectra were measured by a P45X potentiostat-galvanostat with an FRA module. Current-voltage (I-V) characteristics of solar devices were measured with PVIV-1A I-V Test Station under the light illumination from Sol3A Class AAA Solar Simulator (Newport).

Results and Discussion

Structural analysis of the prepared films

Figure 2 shows the top and cross sectional SEM images of perovskite thin films deposited at different spin-coating speeds. As can be seen from SEM images, the surface morphology of the perovskite filmsvaries with increasing the rotation speed (Figures 2a-2c). At lower speeds (2000-4000 rpm), films have irregular grain sizes and have high roughness. At higher speeds, the distribution of grain sizes becomes significantly narrower and it is noticeable that films become smoother (more flat) (Figure 2d-e). Figure 2f shows the dependence of the thickness of the perovskite films on the rotation speed. As it was expected the film thickness decreases with increasing in the rotation speed.

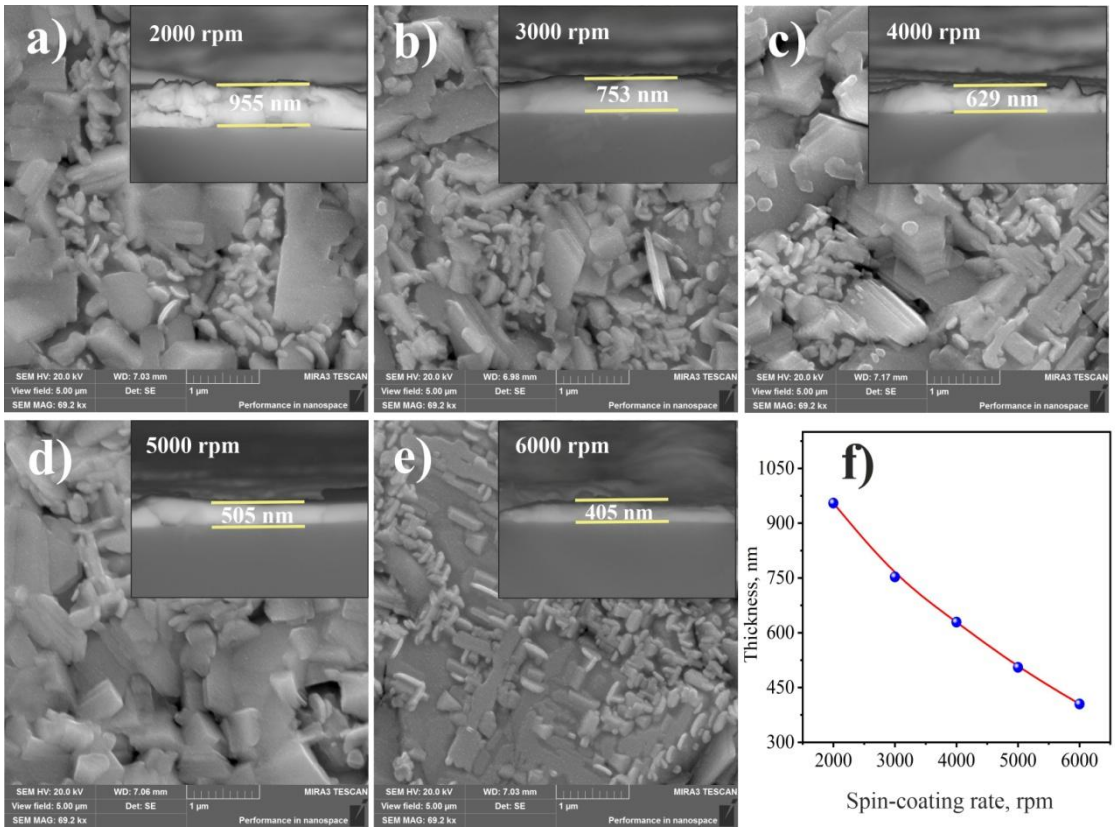

Figure2. SEM images of perovskite films deposited at different spin speeds (a-e) and their thicknesses (f).

Figure 3 shows the AFM images of perovskite films deposited at different rotation speeds. The AFM images are consistent with SEM data. In general, the film roughness decreases as spin-coating rotation speed increases. The observed pores in the films are associated with the evaporation of the solvent during the drying of the films. With an increase in the rotation speed, a structure appears on the surface of the film with characteristic sizes of regions of several hundred nanometers (Figures 3a-3e). The appearance of such a structure can be explained by the FTO substrate surface influence.

Figure 3f shows the dependence of the film surface roughness (RMS) on the rotation speed. As it was expected the surface roughness falls as the rotation speed increases. However, it should be noted that we observe a slight growth in thoroughness at 6000 rpm (Table 1).

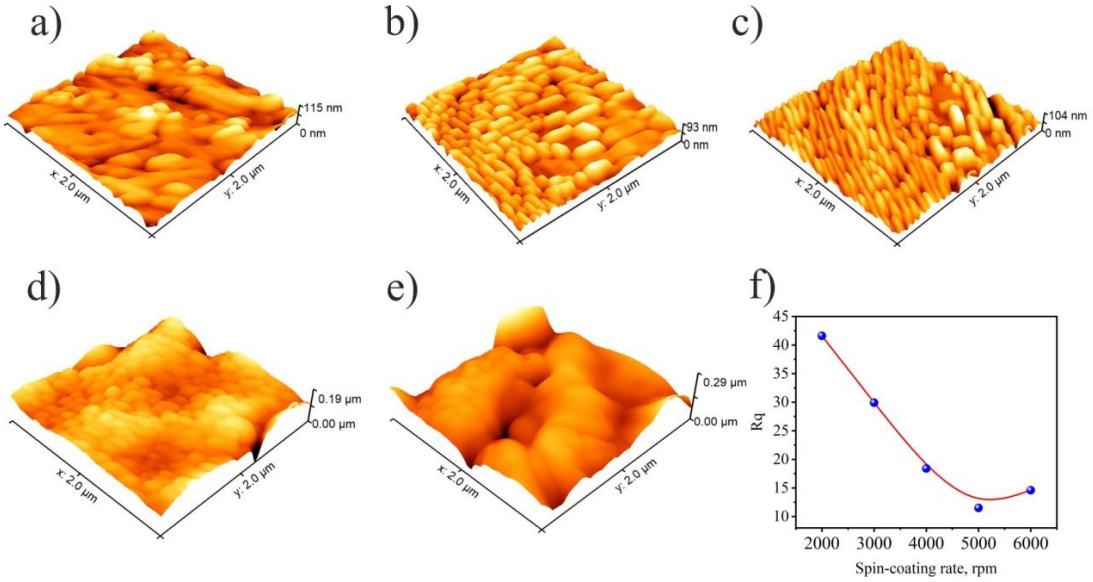

a) 2000 rpm.; b) 3000 rpm.; c) 4000 rpm.; d) 5000 rpm.; e) 6000 rpm.

Figure 3. AFM images of perovskite thin films deposited at different rotation speeds

Table 1

Perovskite film roughness and components surface size

Spin-coating rate, rpm	Layer thickness (t), nm	R_q, nm	$D_{ave.}$, nm
2000	955	41.6	200
3000	753	29.9	220
4000	629	18.4	250
5000	505	11.5	162
6000	405	14.6	120

Optical properties

Figure 4a shows the absorption spectra of the $CH_3NH_3PbCl_xI_{3-x}$ photoactive layer. That's seen from the obtained spectra, absorptions are located at 300 — 700 nm. As known, $CH_3NH_3PbCl_xI_{3-x}$ is a well-absorbing photocell, which has strong absorption in the visible ranges [23, 24]. When measuring the absorption spectra of $CH_3NH_3PbCl_xI_{3-x}$. it was found that with increasing thickness, the maximum of the absorption spectrum shifts from the short-wavelength to the long-wavelength region λ_{max}= 478 nm at a thickness of 400 nm, λ_{max}= 519 nm at a thickness of 505 nm, λ_{max} = 524 nm at a thickness of 640 nm, λ_{max}= 540 nm at a thickness of 753 nm, λ_{max}= 630 nm at a thickness of 955 nm. This shift to the short wavelength region is associated with a change in the surface structure of the $CH_3NH_3PbCl_xI_{3-x}$ films. Figure 4c shows the luminescence spectra of $CH_3NH_3PbCl_xI_{3-x}$ films with different thicknesses. As can be seen from the figure, when $CH_3NH_3PbCl_xI_{3-x}$ films are photoexcited at a wavelength of 650 nm, changes in the luminescence intensity are observed. The maximum luminescence intensity of $CH_3NH_3PbCl_xI_{3-x}$ films with a thickness of 955 nm was observed at 773 nm (1.6 eV).

For $CH_3NH_3PbCl_xI_{3-x}$ films with a thickness of 955 nm, a luminescence peak is observed at a wavelength of λ_{max}= 773 nm and a spectral half-width of FWHM λ=53 nm; 773 nm and spectral half-width FWHM λ=50 nm, films with a thickness of 505 nm are observed λ_{max}= 773 nm and spectral half-width FWHM λ=51 nm, films with a thickness of 405 nm are seen λ_{max}= 774 nm and spectral half-width FWHM λ=51 nm. The band gap was calculated from the intrinsic absorption edge of the UV and visible spectra. The band gap of the $CH_3NH_3PbCl_xI_{3-x}$ films was estimated using the Tauc Plot method. As can be seen from the figure, the $CH_3NH_3PbCl_xI_{3-x}$ film with a thickness of 405 nm has a band gap of about E_g=1.57 eV. With an increase in film thickness from 505 and 629 nm, an increase in the band gap of $CH_3NH_3PbCl_xI_{3-x}$ films is observed, respectively, E_g=1.58 eV and E_g=1.59 eV. A further increase in the thickness of the films 753 and 955 nm does not change the band gap E_g=1.57 eV (Figure 4b). Optical characteristics of $CH_3NH_3PbCl_xI_{3-x}$ films are presented in Table 2.

For hybrid (X = I, Cl) perovskite (Fig. 4a), the optical absorption band between 2.5 and 2.7 eV is due to the Pb-Pb intracomponent transition. When these transitions are further separated into the most important contributions of angular particles, the results show that these transitions mainly came from s (Pb)-p (Pb) and with a smaller proportion of s (I) -p(I) and p(Pb)- p(I). Following our results, this band was attributed [25] to the transition from Pb2+(6s) to Pb2+(6p). Our results also agree with the results of [26], in which three peaks appear in the absorption spectra at approximately 1.65, 2.20, and 3.10 eV. The first peak at about 1.65 eV is mainly associated with the excitation of s(Pb)-p(Pb). The second, with a maximum of about 2.20 eV, is also mainly due to the s(Pb)-p(Pb) transitions with a smaller contribution from the s(I)-p(I) excitation. The last peak at about 3.10 eV is due to similar contributions from s (Pb)-p (Pb), s (I)-p (I), and p (Pb)-p (I).

Further, we studied the dynamics of the perovskite quality and crystallization process depending on photoactive layer thickness by observing the photoluminescence spectra of the perovskite. In Figure 4c photoluminescence spectra of perovskite layers deposited on glass substrates with various photoactive layer thicknesses are illustrated. The photoluminescence band of the perovskite has a maximum at λ_{max} = 785 nm. As seen in PL spectra, the luminescence intensity of the perovskite layer deposited on the spin rate at 5000 rpm had the highest PL intensity. It has indicated that the photoactive layers' best quality and crystallization rate reached a thickness of 505 nm.

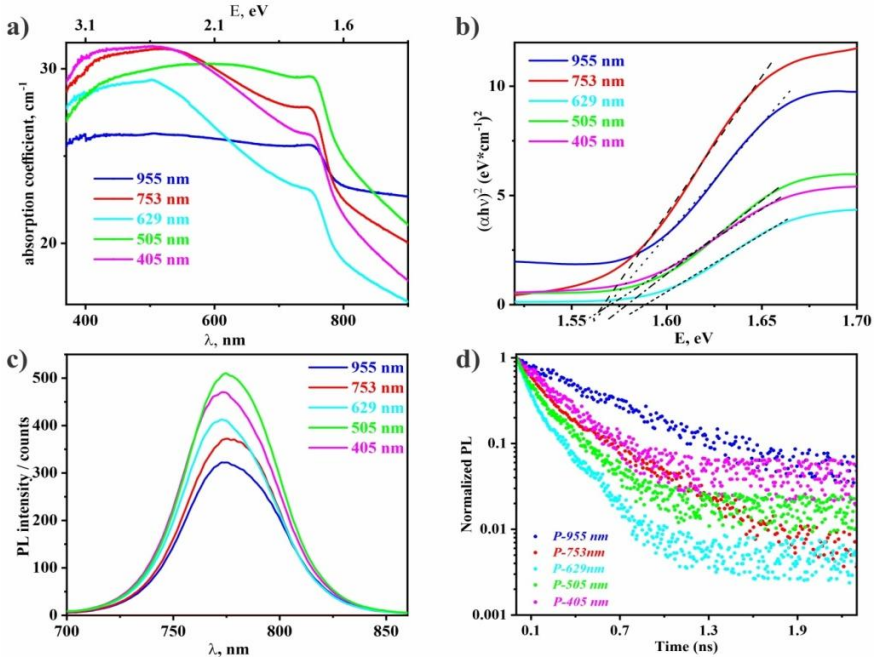

Figure 4. Perovskite films absorbance coefficient (a), optical bandgap (b), PL spectra (c), and TRPL decay plot (d)

We studied the dynamics of charge transfer from a perovskite layer to ETL and how the charge transfer depends on photoactive layer thickness by the time-resolved photoluminescence (TRPL) technique was used to compare PL intensity decays and evaluate PL lifetimes (τ_{PL}) in the perovskite layers with different thicknesses deposited on TiO_2 layer. As seen from TRPL (Figure 4d) and Table 2, the PL intensity decay occurs faster in the perovskite layer with a thickness of 505 nm. Similarly with the PL intensity quenching, at

first, PL lifetime decreases with reducing perovskite layer thickness reaching a minimum value of ~0.8 ns at a perovskite layer thickness of 505 nm, which confirms that effective charge transfer occurs from the perovskite into ETL at the perovskite layer thickness of ~ 500 nm. However, at the lower thickness, the thickness decay time increases indicating the worsened charge transfer.

Table 2

PL, optical bandgap, and TRPL characteristics

t, nm	Maximum PL λ, nm	FWHM λ, nm	Bandgap, eV	τ_{PL}, ns
955	772.66	52.93	1.57	2.3
753	775.49	50.42	1.57	1.9
629	772.66	50.01	1.58	1.1
505	773.23	51.31	1.59	0.8
405	774.36	50.05	1.57	1.0

Photoelectrical characterizations

The current-voltage characteristics and the energy diagram of the components of perovskite solar cells are shown in Figure 5. Figure 5a shows that PSCs with $CH_3NH_3PbCl_xI_{3-x}$ films at a deposition rate of 2000 rpm have the worst photovoltaic parameters, which are due to a low fill factor (FF) of 47.27 %. Cells with $CH_3NH_3PbCl_xI_{3-x}$ films obtained at rotation speeds of 3000 rpm, 4000 rpm, and 6000 rpm show the best solar-to-electrical energy conversion efficiency, which are η=7.93 %, η=8.83 %, and η=8.67 %, respectively, compared to the efficiency of PSCs at 2000 rpm (η=7.13 %). The maximum value of the increase in the CVC parameters is observed for the composite cell obtained at rotation speeds of 5000 rpm, the short circuit current density (J_{sc}) increased by 30 %, and the efficiency value was 9.92 %.

The energy diagram was constructed according to the data from [25, 26]. According to these works, the position of the valence band maximum (VBM) of TiO_2 is 4.0 eV, $CH_3NH_3PbCl_xI_{3-x}$ is 5.4 eV, the VBM for MoO_3 films is 5.38 eV, and for CuPc films the VBM is 5.2 eV. As can be seen from the diagram, the energy levels of the $CH_3NH_3PbCl_xI_{3-x}$ and CuPc MIGs are in good agreement, which should ensure efficient injection of holes from the photoactive layer (PS) into CuPc. The CVC parameters of solar cells are given in Table 3.

However, it is not limited and further optimization is needed to boost photovoltaic performance and eliminate hysteresis (Fig. 5b). We also studied the reproducibility of the PCE of our devices. It fabricated 10 devices for each type of PSC under the same conditions. Figure 5c shows the statistical deviation of PCE from the average value.

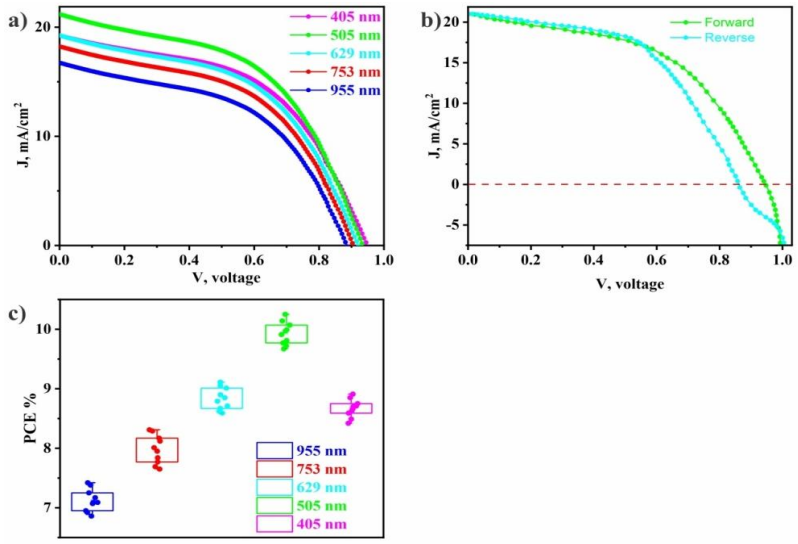

Figure 5. Current-voltage characteristics of perovskite solar cells a), current-voltage characteristics of the champion device for forward and reverse scans b), and PCE statistics c)

Table 3

Parameters of current-voltage characteristics of perovskite solar cells

t, nm	J_{sc} mA/см^2	U_{oc} V	J_{max} mA/см^2	U_{max} V	*FF* %	η %
955	16.96	0.89	11.69	0.61	47.27	7.13
753	18.14	0.90	12.67	0.63	48.87	7.98
629	19.33	0.92	13.58	0.65	48.05	8.83
505	20.76	0.94	15.04	0.66	50.82	9.92
405	19.14	0.95	13.55	0.64	47.68	8.67

To understand the effects of perovskite thickness and defects on charge transfer processes, we used the impedance spectroscopy (IS) technique. IS responses of PSCs were measured in the dark at 0.8 V. In Figure 6 (a) IS spectra in Nyquist coordinates are presented. Dotted and solid lines represent the measured and fitted data, respectively. Overall, in IS spectra we observe two semicircles, one in a high-frequency (HF) region and another in a low-frequency (LF) region. Nowadays, the interpretation of IS spectra of PSCs is controversial [25–27], however, it is accepted that HF is attributed to charge transfer processes in PCSs, whereas R_3C_3 is related to electrochemical processes inside the perovskite layer.

The equivalent circuit shown in Figure 6 (a (insert)) was used to fit IS spectra. According to the works [28], R_1 is a series resistance of charge collectors ETL and hole collectors HTL. R_2C_2 characterizes perovskite/selective contact interfaces, and R_3C_3 is attributed to the slow electrochemical processes inside the perovskite absorber. We are interested in R_1 and R_2 due to these two resistances reflect the effect of perovskite thickness and R_3 reflects the electrochemical processes defects on charge transfer processes. In our work, all functional layers of PSCs, except the perovskite layer, were deposited under the same conditions and for this reason, the changes of R_1, R_2, and R_3 values are related significantly with changes of perovskite properties and HTL/perovskite/ETL interface quality.

Parameters affecting charge transfer processes in PSCs estimated from IS spectra are presented in Table 4. As seen from Table 4, with the reduction of perovskite thickness R_1 becomes lower by reaching a minimum value of 24.3 Ohms at the thickness of 505 nm, and with further thickness decrease it starts to grow. This trend in R_1 is consistent with trends in J_{SC} and FF confirming that by decreasing perovskite layer thickness, HTL/perovskite/ETL interface resistance should decrease, however, the increase of the intrinsic ionic defects density, observed from the absorbance and luminescence study, oppositely influences series R_1 resistance. The two competitive charge transport processes take place in perovskite: electron transport through the $CH_3NH_3PbCl_xI_{3-x}$ conduction band and electron trapping by deep trap levels formed by $CH_3NH_3PbCl_xI_{3-x}^+$ species. Therefore according to the IV and IS studies, the ideal $CH_3NH_3PbCl_xI_{3-x}$ layer thickness at which there is a balance between that competitive photo conversation and charge transport processes is about 505 nm for our deposition condition.

R_2 determines the charge transfer rate at the HLT/perovskite/ETL interface. We observe the increase of R_2, which imply on the electron–hole separation increases with the $CH_3NH_3I_3PbCl_x$ thickness reduction. The charge transfer rate at perovskite/ETL interface depends on the energy level alignment. As seen from Table 2, the decrease of $CH_3NH_3PbClxI_{3-x}$ layer thickness results to widening of $CH_3NH_3PbClxI_{3-x}$ bandgap, which may be due to the rise of the electron quasi-Fermi level. When $CH_3NH_3PbClxI_{3-x}$ electron quasi-Fermi level approaches the perovskite conduction band level the drive force becomes stronger and this will increase the electron transport rate. Additionally, R_2 increase can be associated with the decrease of the recombination rate in perovskite layer. R_3 decrease is associated with the decreased density of $CH_3NH_3PbCl_xI_{3-x}^+$ — related defects, which can form electron trap levels for the electron–hole separation.

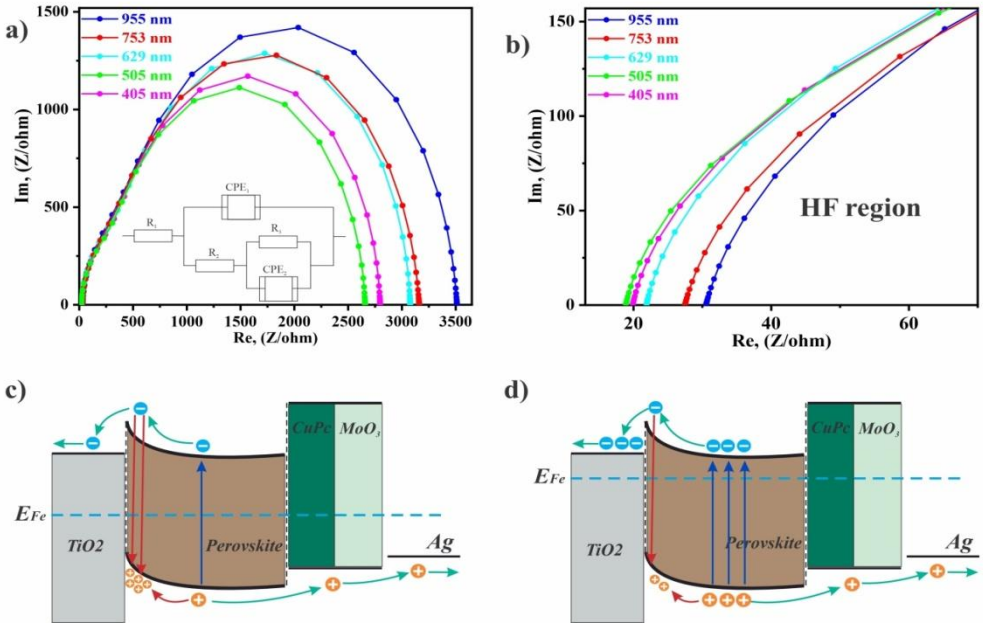

Figure 6. Nyquist impedance curves and equivalent circuit diagrams (insert) (a), increased high-frequency region curves (b), and photocurrent transformation and recombination mechanisms for perovskite solar cells(c), (d)

Figure 6c, d shows the PSCs' photocurrent transformation and recombination mechanisms. As seen in the figure, the sample illuminated electron-hole pairs that were photo-generated inside $CH_3NH_3PbCl_xI_{3-x}$(blue arrow). The holes are transferred to CuPc with MoO_3 (HTL), then transported to the metal contact. While the electrons are moving towards the TiO_2 (ETL), a consequence of the tunnel injection, the electrons will be transferred to the FTO, thus generating a current. However, perovskites have intrinsic ionic defects as iodine ions immigrate rapidly under operating conditions and accumulate at the TiO_2/perovskite interface because of the self-doping effect. These ions explain the trap levels near the valence band, where photo-generated holes accumulations to attract recombination (green arrows).

Decreasing the photoactive layer thickness to 505 nm leads to increases in the graduate of $CH_3NH_3PbCl_xI_{3-x}$ crystals. The increase in crystal size and graduates was the reduction of grain boundaries, which act as the source of mobile defects. Therefore, the light absorption cross-section increases, increasing photo generation and directly improving J_{sc}. Then, recombination decreases at the outer boundaries, resulting in a higher ability to accumulate electrons in the conduction band, which leads to an upward shift in the electron quasi-Fermi level and an increase in V_{oc} (see Figure 6 d). As a result, improving the quality of the TiO_2/perovskite film interface and perovskite/CuPc-MoO_3 films interface leads to a reduction in leak sources, which leads to an increase in FF. Thus, the quality of the photoactive layer simultaneously improves three photovoltaic parameters, which leads to a significant increase in photo conversion efficiency. The exponent n defines the deviation from the capacity ideal behavior and is related to the angle θ, p-capacity. Moreover, for n = 1, p has Farad units indicating that CPE behaves as an ideal capacitor.

Table 4

The value of charge transport parameters of perovskite solar cells

Thickness photoactive layer, nm	**R_s, Ω**	**R_2, Ω**	**R_3, Ω**	p_1	n_1	p_2	n_2
955	30.5	880	2590	$3\cdot10^{-9}$	0.95	$2.4\cdot10^{-8}$	0.93
753	27.5	915	2258	$6.2\cdot10^{-9}$	0.96	$5.7\cdot10^{-8}$	0.88
629	25.9	1003	1779	$2.6\cdot10^{-8}$	0.98	$4.5\cdot10^{-8}$	0.91
505	24.3	1069	1547	$2.5\cdot10^{-7}$	0.98	$1.6\cdot10^{-7}$	0.95
405	29.9	1051	1969	$1.3\cdot10^{-7}$	0.93	$9.1\cdot10^{-7}$	0.96

Conclusions

$CH_3NH_3PbCl_xI_{3-x}$ perovskite films were deposited by spin-coating technique from a methylammonium iodide (MAI) and lead chloride ($PbCl_2$) solution. The effect of the spin-coating rate on $CH_3NH_3PbCl_xI_{3-x}$ thickness and surface roughness was investigated. The $CH_3NH_3PbCl_xI_{3-x}$ films were used as photoactive layers for perovskite solar cells (FTO/TiO_2/$CH_3NH_3PbCl_xI_{3-x}$/CuPc/MoO_x/Ag). The deposition conditions of $CH_3NH_3PbCl_xI_{3-x}$ layer affect recombination resistance in PSCs. We observed two competitive effects on the $CH_3NH_3PbCl_xI_{3-x}$ resistance. As expected, the elevation of the spin-coating rate resulted in $CH_3NH_3PbCl_xI_{3-x}$ thickness reduction, which should lead to a decrease in $CH_3NH_3PbCl_xI_{3-x}R_3$ resistance. However, the impedance spectroscopy revealed that with thickness reduction from 955 nm to 753 nm, the R_3resistance of $CH_3NH_3PbCl_xI_{3-x}$ declines from about 2590Ω to 2258Ω reaching the minimum value at 505 nm. The further decrease in $CH_3NH_3PbCl_xI_{3-x}$ thickness increased $CH_3NH_3PbCl_xI_{3-x}$ film resistance. The study of $CH_3NH_3PbCl_xI_{3-x}$ absorbance and luminescence spectra showed that the change in $CH_3NH_3PbCl_xI_{3-x}$ defect density occurred, which explains the decrease in $CH_3NH_3PbCl_xI_{3-x}$ resistance. According to the absorbance and luminescence spectroscopy study, the $CH_3NH_3PbCl_xI_{3-x}$ thickness reduction led to a decrease in the density of interstitial $CH_3NH_3PbCl_xI_{3-x}^+$ defects. $CH_3NH_3PbCl_xI_{3-x}^+$ species form deep levels trapping free electrons and as a result, increasing $CH_3NH_3I_3PbCl_x$ resistance. The PSCs based on a 505 nm thick $CH_3NH_3PbCl_xI_{3-x}$ layer showed the highest performance with the improved short current density and fill factor. The champion device had a power conversion efficiency of 9.92 %. This work revealed that two competitive charge transport processes occur in $CH_3NH_3PbCl_xI_{3-x}$photoactive layer: electron transport through the $CH_3NH_3PbCl_xI_{3-x}$ conduction band and electron trapping by deep trap levels formed by $CH_3NH_3PbCl_xI_{3-x}^+$ species. The balance between these charge transport processes is about 505 nm for our deposition condition.

Acknowledgments

This research is funded by the Science Committee of the Ministry of Science and Higher Education of the Republic of Kazakhstan (Grant No. AP13067629).

References

1 Kojima, A., Teshima, K., Shirai, Y. & Miyasaka, T. (2009). Organometal Halide Perovskites as Visible-Light Sensitizers for Photovoltaic Cells, *J. Am. Chem. Soc.*, *131*, 6050-6051. https://doi.org/10.1021/ja809598r.

2 Bi, D., El-Zohry, A. M., Hagfeldt, A. & Boschloo, G. (2014). Improved Morphology Control Using a Modified Two-Step Method for Efficient Perovskite Solar Cells, *ACS Appl. Mater. Interfaces*, *6*, 18751-18757. https://doi.org/10.1021/am504320h.

3 Bi, D., Moon, S.-J., Häggman, L., Boschloo, G., Yang, L., Johansson, E.M.J., Nazeeruddin, M.K., Grätzel, M. & Hagfeldt, A. (2013). Using a two-step deposition technique to prepare perovskite ($CH_3NH_3PbI_3$) for thin film solar cells based on ZrO_2 and TiO_2mesostructures, *RSC Adv.*, *3*, 18762-18766. https://doi.org/10.1039/C3RA43228A

4 Jeon, N.J., Noh, J.H., Yang, W.S., Kim, Y.C., Ryu, S., Seo J. & Seok, S.I. (2015). Compositional engineering of perovskite materials for high-performance solar cells, *Nature*, *517*, 476-480. https://doi.org/10.1038/nature14133.

5 Yang, W. S., Park, B.-W., Jung, E. H., Jeon, N.J., Kim, Y.C., Lee, D.U., Shin, S.S., Seo, J., Kim, E.K., Noh, J.H. & Seok, S.I. (2017). Iodide management in formamidinium-lead-halide–based perovskite layers for efficient solar cells, *Science*, *356*, 1376-1379. https://doi.org/10.1126/science.aan2301.

6 Burschka, J., Pellet, N., Moon, S. J., Humphry-Baker, R., Gao, P., Nazeeruddin M.K. & Gratzel, M. (2013). Sequential deposition as a route to high-performance perovskite-sensitized solar cells, *Nature*, *499*, 316-319. https://doi.org/10.1038/nature12340

7 Chen, Q., Zhou, H., Hong, Z., Luo, S., Duan, H.S., Wang, H.H., Liu, Y., Li, G. & Yang, Y. (2014). Interface engineering of highly efficient perovskite solar cells, *J. Am. Chem. Soc.*, *136*, 622-625. https://doi.org/10.1021/ja411509g

8 Snaith, H.J. (2013). Perovskites: The Emergence of a New Era for Low-Cost, High-Efficiency Solar Cells. *J. Phys. Chem. Lett.*, *4*, 3623-3630. https://doi.org/10.1021/jz4020162

9 Choi, K., Lee, J., Kim, H.I., Park, C.W., Kim, G., Choi, H., Park, S., Park, S.A. & Park, T. (2018). Thermally stable, planar hybrid perovskite solar cells with high efficiency, *Energy Environ. Sci.*, *11*, 3238-3247.https://doi.org/10.1039/C8EE02242A

10 Correa-Baena, J.P., Abate, A., Saliba, M., Tress, W., Jacobsson, T.J., Gratzel, M. & Hagfeldt, A. (2017). The rapid evolution of highly efficient perovskite solar cells, *Energy Environ. Sci.*, *10*, 710-727. https://doi.org/10.1039/C6EE03397K

11 Dubey, A., Adhikari, N., Mabrouk, S., Wu, F., Chen, K., Yang, S. & Qiao, Q. (2018). A strategic review on processing routes towards highly efficient perovskite solar cells, *J. Mater. Chem. A*, *6*, 2406-2431. https://doi.org/10.1039/C7TA08277K

12 Stolterfoht, M., Grischek, M., Caprioglio, P., Wolff, C. M., Gutierrez-Partida, E., Pena-Camargo, F., Rothhardt, D., Zhang, S., Raoufi, M., Wolansky, J., Abdi-Jalebi, M., Stranks, S. D., Albrecht, S., Kirchartz, T. & Neher, D. (2020). How To Quantify the

Efficiency Potential of Neat Perovskite Films: Perovskite Semiconductors with an Implied Efficiency Exceeding 28, *Adv Mater.*, *32*(17), 2000080. https://doi.org/10.1002/adma.202000080

13 Lu, J., Lin, X., Jiao, X., Gengenbach, T., Scully, A.D., Jiang, L., Tan, B., Sun, J., Li, B., Pai, N., Bach, U., Simonov, A.N. & Cheng, Y.-B. (2018). Interfacial benzenethiol modification facilitates charge transfer and improves stability of cm-sized metal halide perovskite solar cells with up to 20 % efficiency, *Energy Environ. Sci.*, *11*, 1880-1889. https://doi.org/10.1039/C8EE00754C

14 Wu, Z., Liu, Z., Hu, Z., Hawash, Z., Qiu, L., Jiang, Y., Ono, L.K. & Qi, Y. (2019). Highly Efficient and Stable Perovskite Solar Cells via Modification of Energy Levels at the Perovskite/Carbon Electrode Interface, *Adv. Mater.*, *31*, e1804284. https://doi.org/10.1002/adma.201804284

15 Christians, J.A., Schulz, P., Tinkham, J.S., Schloemer, T.H., Harvey, S.P., de Villers, B. J.T., Sellinger, A., Berry, J.J. & Luther, J.M. (2018). Tailored interfaces of unencapsulated perovskite solar cells for >1,000 hour operational stability, *Nat. Energy*, *3*, 68-74. https://doi.org/10.1038/s41560-017-0067-y

16 Feng, M., You, S., Cheng, N. & Du, J. (2019). High quality perovskite film solar cell using methanol as additive with 19.5 % power conversion efficiency, *Electrochim. Acta*, *293*, 356-363. https://doi.org/10.1016/j.electacta.2018.09.195

17 Jamal, M.S., Bashar, M.S., Hasan, A.K.M., Almutairi, Z.A., Alharbi, H.F., Alharthi, N.H., Karim, M.R., Misran, H., Amin, N., Sopian, K.B. & Akhtaruzzaman, M. (2018). Fabrication techniques and morphological analysis of perovskite absorber layer for high-efficiency perovskite solar cell: A review, *Renew. Sust.Energ. Rev.*, *98*, 469-488. https://doi.org/10.1016/j.rser.2018.09.016

18 Li, Y., Ji, L., Liu, R., Zhang, C., Mak, C.H., Zou, X., Shen, H.-H., Leu, S.-Y. & Hsu, H.-Y. (2018). A review on morphology engineering for highly efficient and stable hybrid perovskite solar cells, *J. Mater. Chem. A*, *6*, 12842-12875. https://doi.org/10.1039/C8TA04120B

19 AbdMutalib, M., Aziz, F., Ismail, A.F., Wan Salleh, W.N., Yusof, N., Jaafar, J., Soga, T., Sahdan, M.Z. & Ludin, N.A. (2018). Towards high performance perovskite solar cells: A review of morphological control and HTM development, *Appl. Mater. Today*, *13*, 69-82. https://doi.org/10.1016/j.apmt.2018.08.006

20 Kim, H.S., Hagfeldt, A. & Park, N.G. (2019). Morphological and compositional progress in halide perovskite solar cells, *Chem. Commun.*, *55*, 1192-1200. https://doi.org/10.1039/C8CC08653B

21 Guo, Q., Yuan, F., Zhang, B., Zhou, S., Zhang, J., Bai, Y., Fan, L., Hayat, T., Alsaedi A. & Tan, Z. (2018). Passivation of the grain boundaries of $CH_3NH_3PbI_3$ using carbon quantum dots for highly efficient perovskite solar cells with excellent environmental stability, *Nanoscale*, *11*, 115-124. https://doi.org/10.1039/C8NR08295B

22 van Franeker, J.J., Hendriks, K.H., Bruijnaers, B.J., Verhoeven, M.W.G.M., Wienk, M.M. & Janssen, R.A.J. (2017). Monitoring Thermal Annealing of Perovskite Solar Cells with In Situ Photoluminescence, *Adv. Energy Mater.*, *7*, 1601822. https://doi.org/10.1002/aenm.201601822

23 Agiorgousis, M.L., Sun, Y.Y., Zeng, H. & Zhang, S. (2014). Strong covalency-inducedrecombination centers in perovskite solar cell material $CH_3NH_3PbI_3$, *J. Am. Chem. Soc. 136*(41), 14570-14575. https://doi.org/10.1021/ja5079305

24 Fu, Y., Song, Q., Lin, T., Wang, Y., Sun, X., Su, Z., Chu, B., Jin, F., Zhao, H., Li, W. & Lee, C.S. (2017). High performance photomultiplication perovskite photodetectors with PC60BM and NPB as the interlayers, *Organic Electronics*, *51*, 200-206. https://doi.org/10.1016/j.orgel.2017.09.028

25 Hirasawa, M., Ishihara, T. & Goto, T. (1994). Exciton features in 0-, 2-, and 3-dimensional networks of [PbI6]4- octahedra, *J. Phys. Soc. Jpn.*, *63*, 3870-3879. https://doi.org/10.1143/JPSJ.63.3870

26 Im, J.-H., Lee, C.-R., Lee, J.-W., Park, S.-W. & Park, N.-G. (2011). 6.5 % efficient perovskite quantum-dot-sensitized solar cell, *Nanoscale*, *3*, 4088-4093, https://doi.org/10.1039/C1NR10867K

27 Yang, T., Wang, M., Cao, Y., Huang, F., Huang, L., Peng, J., Gong, X., Cheng, S.Z.D. & Cao, Y. (2012). Polymer Solar Cells with a Low-Temperature-Annealed Sol–Gel-Derived MoOx Film as a Hole Extraction Layer, *Adv. Energy Mater.*, *2*, 523-527. https://doi.org/10.1002/aenm.201100598

28 Wang, S., Sakurai, T., Wen, W. & Qi, Y. (2018). Energy Level Alignment at Interfaces in Metal Halide Perovskite Solar Cells, *Adv. Mater. Interfaces*, *5*(22), 1800260.https://doi.org/10.1002/admi.201800260

Т.М. Мұқаметқали, К.С. Рожкова, А.К. Аймуханов, Б.Р. Ильясов,
К. Апше, А.К. Зейниденов

$CH_3NH_3PbCl_xI_{3-x}$ перовскит қабатының қалыңдығы және түйіршіктер мөлшерінің электрофизикалық және оптикалық қасиеттеріне әсері

Қорғасын галогенді перовскит $CH_3NH_3PbCl_xI_{3-x}$ пленкалары перовскит күн батареяларында фотоактивті қабаттар ретінде кеңінен қолданылады. $CH_3NH_3PbCl_xI_{3-x}$ -жұтылу спектрі, энергияны түрлендіру тиімділігі және тыйым салынған аймақта өткізгіштігі кең жолақты жартылай өткізгіш, энергияны теңестіру тұрғысынан металлогалидті перовскиттерде жоғары фотоактивті қабатты көрсетеді, бұл электрондарды тасымалдау кезінде зарядтардың тиімді бөлінуін және электрондардың энергияның аз жоғалуын қамтамасыз етеді. Бұл жұмыста $CH_3NH_3PbCl_xI_{3-x}$ қабаттары метиламмоний йодидінен (MAI) және қорғасын хлориді (PbCl2) ерітіндісінен бір сатылы айналдыру әдісімен TiO2 бетіне жағылады. Перовскит ерітіндісін дайындау үшін PbCl2 (Sigma-Oldrich) 230 мг PbCl2 және 394 мг MAI 1 мл N, N-Диметилформамид (Сигма-Олдрих) еріткішінде ерітілді. Күтілгендей, айналдыру

жабыны жылдамдығының жоғарылауы $CH_3NH_3PbCl_xI_{3-x}$ қалыңдығының төмендеуіне әкелді, бұл $CH_3NH_3PbCl_xI_{3-x}$ R3 кедергісінің төмендеуіне әкелуі керек. Дегенмен, кедергі спектроскопиясы қалыңдығы 955 нм-ден 753 нм-ге дейін қысқарған кезде $CH_3NH_3PbCl_xI_{3-x}$ R3 кедергісі шамамен 2590 Ω-дан 2258 Ω-ге дейін төмендеп, 505 нм-де минималды мәнге жететіні анықталды. $CH_3NH_3PbCl_xI_{3-x}$ қалыңдығының одан әрі төмендеуі $CH_3NH_3PbCl_xI_{3-x}$ пленка кедергісін арттырды. $CH_3NH_3PbCl_xI_{3-x}$ жұтылу және люминесценция спектрлерін зерттеу $CH_3NH_3PbCl_xI_{3-x}$ ақаулық тығыздығының өзгеруі орын алғанын көрсетті, бұл $CH_3NH_3PbCl_xI_{3-x}$ кедергісінің төмендеуін түсіндіреді. Абсорбция және люминесценция спектроскопиясының зерттеуіне сәйкес, $CH_3NH_3PbCl_xI_{3-x}$қалыңдығының азаюы интерстициалды $CH_3NH_3PbCl_xI_{3-x}$ + ақауларының тығыздығының төмендеуіне әкелді. $CH_3NH_3PbCl_xI_{3-x}$ + түрлері бос электрондарды ұстайтын терең деңгейлерді құрайды және нәтижесінде $CH_3NH_3PbCl_xI_{3-x}$ кедергісін арттырады. Қалыңдығы 505 нм CH3NH3PbClxI3-x қабатына негізделген PSCs қысқа ток тығыздығы және толтыру коэффициенті жақсартылған ең жоғары өнімділікті көрсетті. Ең жақсы құрылғының қуатты түрлендіру тиімділігі 9,92 % болды.

Кілт сөздер: перовскит күн батареялары, фотоактивті қабат, $CH_3NH_3PbCl_xI_{3-x}$, мыс фталоцианин, йод иондары, импедансометр, электронды тасымалдау қабаты, кемтіктерді тасымалдау қабаты.

Т.М. Мукаметкали, К.С. Рожкова, А.К. Аймуханов, Б.Р. Ильясов,
К. Апше, А.К. Зейниденов

Влияние толщины и размера зерен на электрофизические и оптические свойства перовскитного слоя $CH_3NH_3PbCl_xI_{3-x}$

Пленки перовскита из галогенида свинца $CH_3NH_3PbCl_xI_{3-x}$ широко используются в качестве фотоактивных слоев в перовскитных солнечных элементах. $CH_3NH_3PbCl_xI_{3-x}$ представляет собой полупроводник с более узкой запрещенной зоной с широким спектром поглощения, эффективностью преобразования энергии и проводимостью, демонстрирующий превосходный фотоактивный слой в металлогалогенидных перовскитах с точки зрения выравнивания энергии, обеспечивающего эффективное разделение зарядов и меньшую потерю энергии электронами во время переноса электронов. В настоящей работе слои $CH_3NH_3PbCl_xI_{3-x}$ были нанесены на поверхность TiO_2 методом одноэтапного центрифугирования из раствора иодида метиламмония (MAI) и хлорида свинца ($PbCl_2$). Для приготовления раствора перовскита $PbCl_2$ (Sigma–Aldrich), 230 мг $PbCl_2$ и 394 мг MAI растворяли в 1 мл растворителя N, N-диметилформамида (Sigma–Aldrich). Как и ожидалось, увеличение скорости центрифугирования привело к уменьшению толщины $CH_3NH_3PbCl_xI_{3-x}$, что должно было привести к снижению сопротивления $R_3CH_3NH_3PbCl_xI_{3-x}$. Однако импедансная спектроскопия показала, что при уменьшении толщины с 955 нм до 753 нм сопротивление $R_3CH_3NH_3PbCl_xI_{3-x}$ снижается примерно с 2590 Ом до 2258 Ом, достигая минимального значения при 505 нм. Дальнейшее уменьшение толщины $CH_3NH_3PbCl_xI_{3-x}$ увеличивало сопротивление пленки $CH_3NH_3PbCl_xI_{3-x}$. Изучение спектров поглощения и люминесценции $CH_3NH_3PbCl_xI_{3-x}$ показало, что произошло изменение плотности дефектов $CH_3NH_3PbCl_xI_{3-x}$, что объясняет снижение устойчивости $CH_3NH_3PbCl_xI_{3-x}$. По данным спектров поглощения и люминесценции, уменьшение толщины $CH_3NH_3PbCl_xI_{3-x}$ привело к снижению плотности межузловых дефектов $CH_3NH_3PbCl_xI_{3-x}$+. Частицы $CH_3NH_3PbCl_xI_{3-x}$+ образуют глубокие уровни, захватывающие свободные электроны и, как следствие, увеличивающие сопротивление $CH_3NH_3PbCl_xI_{3-x}$. PSC на основе слоя $CH_3NH_3PbCl_xI_{3-x}$ толщиной 505 нм показали наилучшие характеристики с улучшенными плотностью короткого тока и коэффициентом заполнения: КПД преобразования энергии устройства достигли 9,92 %.

Ключевые слова: перовскитные солнечные элементы, фотоактивный слой, $CH_3NH_3PbCl_xI_{3-x}$, фталоцианин меди, ионы йода, импедансометр, транспортный слой электронов, транспортный слой дырок.